RSC Advances

This article can be cited before page numbers have been issued, to do this please use: U. Buttner, S. Sivashankar, S. Agambayev, Y. Mashraei and K. N. Salama, *RSC Adv.*, 2016, DOI: 10.1039/C6RA13582J.

ROYAL SOCIETY OF CHEMISTRY

www.rsc.org/advances

View Article Online
DOI: 10.1039/C6RA13582J

Flash μ-Fluidics A Rapid Prototyping Method For Fabricating Microfluidic Devices

U. Buttner, S. Sivashankar, S. Agambayaev, Y. Mashraei, K. N. Salama

Computer, Electrical and Mathematical Science and Engineering Division (CEMSE),
King Abdullah University of Science and Technology (KAUST), Thuwal, Saudi Arabia
ulrich.buttner@kaust.edu.sa

Microfluidics has advanced in terms of designs and structures; however, fabrication methods are time-consuming or expensive relative to facility costs and equipment needed. This work demonstrates a fast and economically viable 2D/3D maskless digital light-projection method based on a stereolithography process. Unlike other fabrication methods, one exposure step is used to form the whole device. Flash microfluidics is achieved by incorporating bonding and channel fabrication of complex structures in just 2.5sec to 4sec and by fabricating channel heights between 25μm to 150μm with photopolymer resin. The features of this fabrication technique, such as time and cost saving and easy fabrication, is used to build devices that are mostly needed in microfluidic/ lab-on-chip systems. Due to the fast production method and low initial setup costs, the process could be used for point of care applications.

Introduction

Microfluidics has been applied to a broad spectrum of diverse applications due to the fact that capillary forces in confined spaced channels act on particles suspended in liquids different to the system behavior than in the macro scale. Before it came to be used for detecting chemical and biological threats, microfluidics originated as an analytic tool in the field of spectroscopy. When the genomics explosion started, microfluidics had in important role to play in DNA sequencing(1). Later, microelectronics were integrated with microfluidic devices by utilizing clean-room facilities and standard fabrication techniques. The phrase, “lab on a chip (LOC),” (2) has since become a well-known term in the microfluidic community.

These standard fabrication techniques have changed and developed over the years. To date, many LOC devices have been made with techniques inherited from the semiconductor industry, such as photolithography, thin film deposition, etching, and anodic bonding(3). Henceforth, efforts were made to provide a rapid and robust method for fabricating microfluidic devices. The past decade has brought about a shift to the use of polymers, based on polydimethylsiloxane (PDMS) to glass bonding and silicon wafer bonding to poly-methyl methacrylate (PMMA) bonded microfluidic devices. Micromachining and laser etching on PMMA (4) have become the preferred methods of fabrication for microfluidic devices. Recently, the trend in microfluidic device fabrication is based on flexible laminated polymer sheets that use direct laser writing for PCR applications(5). Microfluidic chip-bonding methods(6) have also been improved through the application of vacuum bonding and thermoplastic solutions. Despite the development of these various techniques, the fabrication(7) of LOC devices with aforementioned techniques are time-consuming or expensive and can be complicated to realize.

LOC devices that are integrated with microelectronics find applications in the sensitive detection of label-free analytes (8) over a broad range of concentrations. Through the use of non-traditional approaches such as adhesive film masking(9), dry-film photoresist (10-12), razor-blade cutting(13, 14), oxygen-free flow lithography (15) and structuring through shape-memory polymers (SMPs)(16, 17), the prototyping of microfluidic channels becomes possible(18, 19). Thin films and surfaces patterned to produce micro- and nano-structured metallic surfaces(20, 21) have been applied mostly to Surface-Enhanced Raman Scattering (SERS) applications(22, 23).

Micrometer-sized dimensions below 50μm in fluidic devices are obtained through photolithographic techniques. Photolithography techniques with thin-film methods have been critical for the incorporation of electrical and fluidic controls in micro-total analysis systems. They have also been essential to the integration of detectors(24-26), waveguides(27), heaters(28, 29), filters(30), optical sources(31, 32) in microfluidic systems(33). There are also lithography techniques that allow the integration of electronics; however, lithography limits the design of microchannels to single-depth planar geometries. While it is also possible to build multistep micro-channels via lithographic techniques, the masks used are expensive and time-consuming. Consequently, a fabrication method is preferred that requires less time, less lab space, and is cost effective.

3D printers are becoming more affordable, and many research groups are working on 3D microchannel fabrication (2, 34-38) with building speeds of 22mm/hr, we target to build devices in a few seconds using this stereolithography fabrication method and demonstrate that a whole device can be fabricated in one exposure. Advanced 3D fabrication methods with O-rings for building modular devices have been demonstrated(35) but, it is still time-consuming. The novelty lies in this fabrication method and not in the lithography process. This one-step fabrication method requires only a few seconds to build a 2D/3D microchannel network. By controlling the amount of resin encapsulated between two surfaces, channel heights can range between 25μm to 150μm at a resolution of around 50μm on an area of 25mm x 25mm. Over larger areas (up to a total area of 40mm x 80mm), a resolution of 150μm is achievable. Imaging and spectroscopy can be achieved by integrating microchannels between two quartz slides. As the magnetic field strength is inversely proportional to the square of the distance between magnets, and due to the thin dimensions of the microfluidic chip, magnetic coupling can be utilized on the inlet and outlet piping to the device. This method, when fabricated with biocompatible resin, can also be used to print microfluidic chips(39) to culture cells.

This work is divided into three sections. In the first section, the basic procedure of the proposed microfluidic fabrication technique and its required materials are discussed in detail. The second section is to determine the resolution and exposure times to evaluate the characteristics of the resin before fabricating the device. In the third section, LOC devices are fabricated to demonstrate the proof of concept of this robust method. We begin by demonstrating the use of a Y-junction channel inlet (using red and green food dye) to form a laminar-flow section in a 2D microfluidic mixer(40). Second, the Y-junction and mixer are combined into a microstructure zone to hold cells or proteins. These agglutinants are captured by the microstructures fabricated via the flash microfluidic (FM) method. We demonstrate

View Article Online
DOI: 10.1039/C6RA13582J

how microchips for mixing and agglutination for complex cell analysis are fabricated, a 2D mixer in conjunction with a combined mixer and micro-pillar capture zone for antigen and antibody (agglutinants) was prepared. Also, we demonstrate a concentration gradient to obtain solutions of gradients, a simple spiral mixer, 3D cross flow mixer and integration of gold electrodes via this fabrication method.

Experimental

Microfluidic Fabrication Method

Microfluidic channels are designed in Windows version seven using Microsoft Windows Paint or Solid-Works program on a 64-bit computer operating system. The images of the microfluidic designs in Solid-Works can be saved in STereoLithography (STL) format and converted for segmentation to an open-source package in Creation Workshop from Envision Labs. The program slices the original 3D design into predetermined segments. The slicing of the 3D STL files into many layers is done according to the thickness of the templates. These are then transformed into 2D cross sections. Sliced templates are imported as Portable Network Graphics (PNG) or Bitmap files into a Kudo3D Titan 1 printer. For our 2D exposure, only one transparent surface is needed to allow the pattern to be transferred. For the fabrication, one layer is used as a mask. This means that you could use a 3D STL image, process it with Creation Workshop, and use one slice to complete the final microfluidic chip. The most important parameter is the focusing of the projector. The detailed fabrication procedure is represented in Figure 1.

As shown in the figure below, a standard drill press with a 0.030" x 1/8" x0.125" diamond drill from UKAM Industrial Superhard Tools is used to drill the inlet and outlet holes into the top glass cover slides. Alternately, use of a CO_2 laser to ablate the inlet and outlet holes to 0.5mm has been found to be less time- consuming. Both methods have been tested and found to work well Figure 1(a). The Spot-E resin is either placed between two 25mm × 25mm poly-methyl methacrylate (PMMA) sheets that already have their inlets and outlets connected, or between glass cover slides, one side of which has pre-drilled inlet and outlet holes Figure 1(b). The device was exposed after the initial alignment of the projected pattern with the inlet and outlet drilled holes of the device Figure 1(c). After exposure, the uncured resin was sucked out using a hose attached to vacuum via a vacuum liquid trap and flushed several times with isopropanol (IPA) as represented in Figure 1(d). It is then cleansed with deionized water to stop any further reaction from occurring. A prototype of the device is shown in Figure 1(e).

When glass cover slides are used, the inlet and outlet pipes can be magnetically coupled[33], as illustrated in Figure 1(f). When two PMMA sheets are used, they are coated with chloroform to improve their adhesion properties before the resin is applied(41). Setting the channel height between the two PMMA surfaces can be accomplished either by using a 100µm thick double-sided tape from 3M or by adding a specific volume of resin, which is discussed further. The exposure time is adjusted to 2.8sec for the Spot-e elastic, which is experimentally determined. A video of device fabrication is shown in supplementary information [S1]

The flash microfluidic setup requires a high-resolution Digital Light-Projection (DLP) projector. The resin contained between the two glass slides is quantified and then placed on a holder at a distance of approximately ten centimeters above the projector. To improve the resolution and obtain finer structures (with a minimum feature size of about 50µm), a convex lens is externally fitted between the projector lens and the microfluidic chip. By adding an additional 100mm focal length convex lens at a distance of 10mm placed perpendicular to the projected light, structures in the range of 50 micrometers were achieved. For calibration purposes, there is a calibration function in the Kudo software, which when activated, displays red perpendicular cross hash lines. The calibration technique can be used for focusing and alignment of the lens. This lens also aids in increasing the intensity of light thereby reducing the time of exposure needed to fabricate a device, but also reduces the curing uniformity and reduces the exposure area. The Acer H6510BD high-resolution projector contains a DLP chip, which is a Digital Micro-mirror Device (DMD). The micro-mirrors replicate the design and project each pixel with a total resolution of 1920 x 1080 pixels.

When the additional convex lens is used between the projector and the exposed substrate, the actual exposure time required is between 2.5sec and 4sec for the Spot-e elastic resin, depending on the thickness of the resin. When the additional lens is not used, then the time of exposure is 6-8sec under same conditions. The channel height depends on the amount of resin used between the two surfaces. After exposure and cleaning, a microfluidic probe station can be used to attach the input and output feeds to complete the chip. Additionally, magnetic coupling is shown as a simple method of connecting to the chip without applying glue. The one-step fabrication is illustrated in Figure 1(g), and the experimental set-up is as shown in Figure 1(h).

The DLP chip includes a digital micro-mirror device (DMD), which is a MEMS device consisting of 5.4 µm or less square mirrors, of which each corresponds to a term known as a pixel. The resolution of the DMD chip is defined by many pixels or mirrors across its surface. This array of micro-mirrors can separately control the intensity of the projected light at each pixel image; thereby the reflected light can polymerize each voxel (volumetric pixel) within a photosensitive resin layer. Micro-mirrors are individually addressed electrostatically and pivot the reflected light across their diagonal length, thus by tilting the reflected light is directed away from the projector lens path.

As a projector lens is designed to view an image on a large screen, the final pixel size is dependent on the total projected area. By moving the projected image surface closer, the image can be refocused until a minimum area is reached. Thereafter focusing will not improve by moving any closer. An optimum area of 40 mm x 80 mm was reached. As our chips were 25mm x 25mm, we added a convex lens to refocus and improve the resolution; however we noticed that this is not ideal. As the resolution improves so does the light intensity in the center area. This causes the resin to cure faster at the center. By encapsulating the resin, the center will be overexposed with respect to the outer edges. For microfluidic devices, where the channel widths are 150 microns and above, there is no need to use the additional lens.

Here Figure 1

View Article Online
DOI: 10.1039/C6RA13582J

Preparation of solutions for the acid base mixing

Phenolphthalein in its native form was obtained in powder form. 1% solution of phenolphthalein is used as an indicator in the experiments. Therefore 1 g of phenolphthalein was dissolved in 50% ethanolic solution and made to 1% indicator solution and stored in an eyedropper bottle. Hydrochloric acid (1 M) was prepared and to 9.90 ml of acidic solution, 10 µl of prepared 1% phenolphthalein was added as an indicator. Sodium Hydroxide (NaOH) 1 M solution was used as a basic solution in the pH test experiment.

Results and discussion,

The fabricated devices can also be integrated with analytical devices that enable fluid handling and quantitative analysis. Such applications are important for potential applications in medicine, healthcare, and environmental monitoring(42). For validation purposes, the resolution of the structures, the penetration depth, and the aspect ratio of the two LOC devices fabricated using two types of resin are discussed in this section. The flash methodology used to obtain these two structures is then compared to older fabrication methods.

Microfluidic applications

We demonstrate that flash microfluidics method is efficient for fabricating various devices such as a spiral mixer, a gradient generator, and 3D cross flow mixer. To reveal the versatility of the method we show that this method can be used to integrate with electrodes. Gold was sputtered on a glass substrate and then laser etched the gold to form electrodes. The channel was built on top of the same surface as shown in Figure 2(a). The spiral microfluidic mixer is an interconnection of two half spirals which are joined at the center(43). The turns in half spirals provide a centrifugal force, which enables the fluid to stretch and causes Dean vortices represented in Figure 2(b). If the resin is not well mixed, then the color pigments settle down and show uneven colors (figure 2(b)). Hence it is recommended that the resin is shaken well before use.

Thirdly, we fabricated a fractal gradient generator(44) that can mix three different fluids. The fluids are combining, mixing and splitting into six different outlets, and different mixing rates are generated in each channel as demonstrated in Figure 2(c). Finally, we demonstrate the cross-flow mixer that is a 3D device requiring three steps of exposure for a single device with a total exposure of 15 sec as shown in Figure 2(d). The first exposure has one side flow, and the second exposure has the opposite cross side flow and the third exposure is to combine the top and bottom exposures using resin. This device allows fluids to have a cross flow to mix efficiently. Thus we can create 3D microstructures as well with the new fabrication method that is much easier and faster compared to other 3D printed microfluidics. In particular, we demonstrate the application of a modified Tesla mixer and a microfluidic chip to capture protein complex that could be used for further analysis.
A passive microfluidic 2D mixer was fabricated and two flow rates were optically evaluated with food dye to demonstrate mixing via a modified Tesla valve design, as described in by Hong et al. (40). Fluids in this mixer will tend to flow close to the angled surface. This is known as the Coanda effect, which is used to guide the fluid so that it collides. Due to the impact of the flow, mixing cells oriented in opposite directions were used to repeat the transverse dispersion. Food-grade dyes of different colors (green and red) were diluted with DI water and used to validate this mixing procedure. Green and red food dyes were diluted with DI water and tested at two different flow rates, as depicted in Figure 2(e) at 0.5µl/min and in Figure 2(f) at 0.2µl/min.
From the figures, it can be seen that the dyes are laminar before they reach the mixing section. The red and green food colorants start to mix in the first and second stages and are finally well mixed at the higher flow rate, as shown in Figure 2(e). Hardly any mixing occurs at the lower flow rate.

To demonstrated device utility, we fabricated, a droplet generator that has two inlets and one outlet. Soya bean oil from Alfa Aesar was introduced from the outer two feeds wherein it pinches the center channel forming droplets. The droplet generation device is shown in Figure 2(h), and a snapshot of the droplet generation is shown in Figure 2(i). It is worth mentioning that for droplet generation the top and bottom layer of the device is preferred to be PMMA as the glass is more hydrophilic and water has a tendency to stick to it, and it is thus more difficult to generate droplets. A video of droplet generation is shown in supplementary information [S2]

To evaluate the resistance of chemicals to resins we performed a simple chemical test. The chemical test involved a reaction between an acid and a base with phenolphthalein as an indicator. Phenolphthalein was added into the acidic solution. At the inlets the solutions are colorless and when the two mix they turn pink as shown in Figure 2(j). The resin shows no damage to its property inferring, and it's inert to the chemical on reacting with these acid or base solutions.

Here Figure 2

CRP agglutination
For point of care applications, a passive agglutination is demonstrated. This is a process in which antibodies are first coated onto latex support and then combined with an antigen to show agglutination. All methods for detecting or quantifying an antigen or antibody take advantage of the fact that they react to form complexes. This phenomenon is specific to CRP. At the optimum antigen-antibody concentration, these complexes precipitate out. FM can fabricate microstructures of various dimensions. To validate the fabrication of microstructures, we demonstrate agglutination on a microfluidic chip and capture the agglutination clumps at the V-shaped structures positioned after the mixer stage. This procedure may have applications in single-cell analysis or drug-delivery systems. The microstructures

View Article Online
DOI: 10.1039/C6RA13582J

are about 100µm and are spaced approximately 100µm apart with a total viewing area of about 2mm^2. Commercially available CRP proteins are diluted with azide buffer. An agglutination experiment was performed to capture the agglutination clumps formed after the interaction between antigen and antibody in the microstructures that are fabricated in the FM methodology, as shown in Figure 3.
However, if an antigen is specific in nature, agglutination of the antigen-antibody complex is observed. The results show that the agglutination complexes are held in the V-shaped structures. The agglutination chip is a proof of concept. It demonstrates that this technology can be applied to more complex structures.

Here Figure 3

Resolution,* Aspect Ratio, *Optimizing exposure penetration depth
Resolution refers to the minimum dimension structure obtained via FM. To obtain the minimum resolution and optimum structure, two patterns are exposed for 3sec with 30µl of Spot-E elastic resin and imaged using the 10x objective lens of a Zeiss Axion microscope, as shown in Figure 4(a-c). A resolution of 49µm has been achieved in an exposed area of 25mm x 25mm with 30µl resin encapsulated. One side is removed, and the side containing the structure is then cleaned with isopropanol (IPA) and measured. There are limitations to this technology in terms of resolution to the total area exposed. The resolution is better near the center than on the outer fringes of a 25mm x 25mm area. Stitching sections would improve the resolution but would require additional hardware. Ideally, an off-the-shelf 3D technology is used, which is easily modified. An Acer H6510BD high-resolution projector used at a resolution of 1920 x 1080 pixels could be further improved by replacing it with the recently launched DLP9000 DMD chip by Texas Instruments at a resolution of 2560 x 1600 pixels.
To determine the aspect ratio of the Spot-e elastic and the FLGPCL02, seven measurements of various resin volumes are performed, each at the same exposure time. The resins are first weighed on a glass cover slide and then encapsulated by adding another glass slide. After a 3sec exposure, the top glass cover slide is removed and the bottom slide containing the structures is washed with IPA and measured using a Tenkor profilometer. A comparison of the two different resins is performed, as represented in Figure 4(d). Spot-e elastic is found to be less viscous, and the clear photopolymer resin FLGPCL02 is more viscous, Spot-e resin shows an increase in height until 66.5mg; thereafter, it stabilizes due to the resin outflow. To counteract this, one would need a construction that is better sealed, but this should make fabrication more complex. The photopolymer FLGPCL02 is comparatively more linear than the Spot-e elastic due to its more viscous composition. With these results, the heights of the channels can be estimated relative to the resin used for this fabrication method.

To understand the exposure rate of the resin used to fabricate the microfluidic devices, an experiment was performed on the Spot-E elastic resin with an open platform. 90mg of resin was spread across a 25mm x 25mm glass cover slide and exposed at time intervals of 0.2sec. At 1sec, little to no photopolymerization was observed. Thus the data was plotted after 1sec to determine exposure time parameters. A Tencor profilometer was used, and measurements were obtained, as plotted in Figure 4(e). There is a non-linear increase in height between 1.1sec and 1.3sec of exposure. After that, the resin cures and the rate of increase in height become more constant and more linear. Intervals of 0.2sec were mapped to determine the penetration depth and energy density, as shown in Figure 4(e). The profile plot of the bonded and unbonded channels obtained from Zeiss Axio microscope is represented in Figure 4(f) and 4(g). Based on these measurements, one can determine the time required to obtain correct curing parameters for specific channel heights. These conditions are specific to the addition of the convex lens used. This is a methodology for determining the penetration depth of resin applied with the specific projector parameters. There is a convex curing profile, which is amplified by using the additional lens. This convex curing profile is due to the projector's intensity profile, which is negligible as the confined resin between the two glass slides is exposed longer to cure the total area. A better performance could be achieved more suitable projector using an LED or Laser as a light source are used and the using beam shaping technique as in (45).

Here Figure 4

Types of Resin
Bench-top 3D printers are the current trend due to a recent to significant cost-reduction. Many resins available in the market are toxic in the liquid form and hence proper health and safety measures should be implemented such as good ventilation and use of gloves and lab coats. And proper MSDS protocol should be addressed. Two different resins are compared: (1) Spot-e elastic, and (2) a clear photopolymer resin, FLGPCL02. Spot-e elastic resin is less viscous and hence can be used for lower channel heights, whereas the more viscous FLGCL02 resin is used for larger channel heights. Both resins are used to show that it is possible to fabricate, for agglutination purposes, a mixer and a combination of a mixer and a bead-trapping zone. However, long-term adhesion and stability tests have not yet been performed. Exposure times are optimized for both resins and two graphs, as shown in Figure 5.
The time required for curing the more viscous FLGPCL02 resin is more than four times that required for the Spot-e elastic clear resin. FLGPCL02 resin also shows that the structures are well defined at higher aspect ratios given a resolution above 100µm.
To determine whether these resins can be applied in thermal reactors for future projects, thermo-gravimetric analysis (TGA) is performed on both resins to determine mass loss over temperatures ranging from room temperature to 800 degrees C. The results (presented in Figure 5) reveal that onset of mass loss occurs at 320 degrees for the Spot-e elastic resin, whereas the onset of mass loss for FLGPCL02 starts earlier at 281 degrees. Both resins may find applications that require heating applications, as in micro reactors.
A pressure test was performed to determine the bonding forces and durability of a sealed microfluidic chip fabricated with our method. In this instance, Kudo Spot Elastic resin was used between the top 1mm PMMA cover cut to 25mm x 25 mm and the bottom 0.180 mm glass

View Article Online
DOI: 10.1039/C6RA13582J

cover slide of the same dimensions. Two 10ml with inner diameter 15.9mm diameter syringes were used with water mixed with food dye. The flow was set to 1ml/min and changed in steps of 1ml/min at 1 min intervals. After reaching 6ml/min delamination on the surface PMMA to resin occurred at one of the inlets. Most of the microfluidic devices are designed to work within this range (1-6 ml/min). Hence we claim it's suitable to build microfluidic device via FM.

Here Figure 5

Effects of Exposure time

The Spot-E elastic resin exposure time is shown in Figure 6. Three exposure times (1sec, 3.7sec, and 30sec) were used, and the effect of the exposed energy on the formation of microstructures is shown. When underexposed (less than 1sec), no solidification or phase change occurs, as illustrated in Figure 6(a). Under optimal exposure, structures are well defined at 3.7sec, as seen in Figure 6(b). This result depends on the width and type of the resin, as discussed earlier. When overexposed (e.g., at 30sec), undefined structures are obtained, as seen in Figure 6(c) where triangular shapes merge and combine to form a rhombus. For the previously mentioned exposures, a convex lens is inserted between the projector and the exposure stage. Once the magnification lens is removed, the time of exposure increases and the dimensions and structure are larger.

Here Figure 6

Existing technologies are compared to the FM fabrication method with respect to fabrication time, resolution, channel depth, and initial setup costs (see table). The more recent 3D printing technology(46) has the advantage of simplicity and low setup costs.
It is difficult to print internal microchannels below 1mm and currently printing rates of 22mm/hr are achievable ([36]), in contrast to the FM method using 2.8sec exposure time and around 2min of flushing a completed microfluidic chip, using the spot-e elastic resin. A further benefit of the FM method is that it is reproducible and that electrodes or sensors are easily integrated without introducing leakages to the LOC.

Table 1: Microfluidic Fabrication Method Comparison Table

Technology	Fabrication Time	Resolution (µm)	Channel Depth (µm)	Initial Setup Costs
3D Printing **(46)**	22mm/hr	250µm	1x2 mm	Low
SU8/Clean room/Maskless Lithography or chrome mask/PDMS casting **(47)**	Speed: 2000µm/sec Casting >1hr	~5µm	>2µm	High
Silicon/glass Bonding/Dry etching/clean room/anodic bonding **(48)**	>4hrs	>1µm	>1µm	High
PDMS casting on laser etch PMMA **(49)**	Speed: 1650 mm/sec Casting >1hr	25µm	>20µm	Medium
PMMA/laser/milling/Thermal bonding **(50)**	Speed: 125mm/sec Bonding >45min	>150µm	>20µm	Medium
Flash Foam mold/PDMS casting **(51)**	Speed: 3–5min Casting >1hr	200µm	~25µm	Low
Direct projection on dry-film photoresist (DP2) **(10)**	> 4hrs	10µm	>10µm	Medium
Flash Microfluidics	***Speed: >2.8sec 2min flushing***	***50µm***	***>10µm***	***Low***

Standard silicone technologies(47, 48) have much better resolutions of around 1µm given channel widths of around 5µm; however, setup costs for the maskless lithography patterning are substantially greater, and it requires a clean room facility. Both SU8 mold fabrication and glass-to-silicon bonding involve additional costs, as the dry-etching system, and bonding equipment is needed. These methods require hours of fabrication time and often need to be trained personnel.Fabricating microfluidic devices that use laser etching, PDMS casting(49, 50) and activated surface bonding are not as costly as the semiconductor technologies mentioned earlier, setup costs would be classed as medium for those technologies. Furthermore, the resolution of channel widths is around 150µm. Fabrication times are also longer than the FM method, which results in more than an hour of fabrication.
More recently, Flash foam was shown(51) to have a good potential to be used as a mold for PDMS casting, as it has a good resolution (of 200µm) and low setup costs. Even here a casting and bonding process is required, which can take up to an hour to fabricate.

View Article Online
DOI: 10.1039/C6RA13582J

In this work, various patterns were made and tested for resolution. A non-cured resin cleaning process was applied to validate the fabrication of a 2D mixer microfluidic chip on its own and to find the ideal flow rate at which mixing would occur. This was followed by consideration of a CRP agglutination chip, which incorporated a 2D mixing stage and a bead-trapping zone.

Conclusions

A fast fabrication method is demonstrated by analyzing a 2D micromixer and a mixer with a capture zone for agglutination assays. The micromixer showed no leakages at flow rates of up to 2µl/min and showed magnetic coupling for inlet and outlet probes. Once the holes are drilled or laser etched on the glass/PMMA slides this procedure requires a cleaning procedure after a single exposure. The amount of resin used can determine the channel height of the chip. The resin is then placed between two surfaces, one being transparent. After one exposure is done, the chip is cleaned and ready to use. By analyzing various technologies, the FM fabrication method has proven to be a fast and low-cost option relative to setup costs, and it has a resolution that is acceptable for microfluidic LOC devices. Furthermore, this method can be used to form solid channels by inverting the image. This process could be used in molds for PDMS casting. Future work will be on optimization and durability testing and on integrating various combinations of textures and standard electronic IC platforms.

References

1. Whitesides GM. The origins and the future of microfluidics. Nature. 2006;442(7101):368-73.
2. Gross BC, Erkal JL, Lockwood SY, Chen C, Spence DM. Evaluation of 3D printing and its potential impact on biotechnology and the chemical sciences. Analytical chemistry. 2014;86(7):3240-53.
3. Sharma H, Nguyen D, Chen A, Lew V, Khine M. Unconventional low-cost fabrication and patterning techniques for point of care diagnostics. Annals of biomedical engineering. 2011;39(4):1313-27.
4. Sivashankar S, Agambayev S, Mashraei Y, Li EQ, Thoroddsen ST, Salama KN. A “twisted” microfluidic mixer suitable for a wide range of flow rate applications. Biomicrofluidics. 2016;10(3):034120.
5. Thompson BL, Ouyang Y, Duarte GR, Carrilho E, Krauss ST, Landers JP. Inexpensive, rapid prototyping of microfluidic devices using overhead transparencies and a laser print, cut and laminate fabrication method. Nature protocols. 2015;10(6):875-86.
6. Cassano CL, Simon AJ, Liu W, Fredrickson C, Fan ZH. Use of vacuum bagging for fabricating thermoplastic microfluidic devices. Lab on a Chip. 2015;15(1):62-6.
7. Lipomi D, Martinez R, Cademartiri L, Whitesides G. 7.11-Soft Lithographic Approaches to Nanofabrication. Polymer Science: A Comprehensive Reference, Ed K Matyjaszewski and M Möller, Elsevier, Amsterdam. 2012.
8. Sivashankar S, Agambayev S, Buttner U and Salama KN, Label-free Detection of Sex determining Region Y (SRY) via Capacitive Biosensor. The 38th Annual International Conference of the IEEE Engineering in Medicine and Biology Society (EMBC’16); 2016 August 16-20; Orlando, Florida USA: IEEE
9. Hancock MJ, Yanagawa F, Jang YH, He J, Kachouie NN, Kaji H, et al. Designer hydrophilic regions regulate droplet shape for controlled surface patterning and 3D microgel synthesis. small. 2012;8(3):393-403.
10. Zhao S, Cong H, Pan T. Direct projection on dry-film photoresist (DP2): do-it-yourself three-dimensional polymer microfluidics. Lab on a Chip. 2009;9(8):1128-32.
11. Tsai Y-C, Jen H-P, Lin K-W, Hsieh Y-Z. Fabrication of microfluidic devices using dry film photoresist for microchip capillary electrophoresis. Journal of Chromatography A. 2006;1111(2):267-71.
12. Leech PW, Wu N, Zhu Y. Application of dry film resist in the fabrication of microfluidic chips for droplet generation. Journal of Micromechanics and Microengineering. 2009;19(6):065019.
13. Bartholomeusz D, Boutté RW, Andrade JD. Xurography: rapid prototyping of microstructures using a cutting plotter. Microelectromechanical Systems, Journal of. 2005;14(6):1364-74.
14. Greer J, Sundberg SO, Wittwer CT, Gale BK. Comparison of glass etching to xurography prototyping of microfluidic channels for DNA melting analysis. Journal of Micromechanics and Microengineering. 2007;17(12):2407.
15. Bong KW, Xu J, Kim J-H, Chapin SC, Strano MS, Gleason KK, et al. Non-polydimethylsiloxane devices for oxygen-free flow lithography. Nat Commun. 2012;3:805.
16. Grimes A, Breslauer DN, Long M, Pegan J, Lee LP, Khine M. Shrinky-Dink microfluidics: rapid generation of deep and rounded patterns. Lab on a Chip. 2008;8(1):170-2.
17. Abdelgawad M, Watson MW, Young EW, Mudrik JM, Ungrin MD, Wheeler AR. Soft lithography: masters on demand. Lab on a Chip. 2008;8(8):1379-85.
18. Kitson PJ, Rosnes MH, Sans V, Dragone V, Cronin L. Configurable 3D-Printed millifluidic and microfluidic ‘lab on a chip’reactionware devices. Lab on a Chip. 2012;12(18):3267-71.

View Article Online
DOI: 10.1039/C6RA13582J

19. Yuen PK, DeRosa ME. Flexible microfluidic devices with three-dimensional interconnected microporous walls for gas and liquid applications. Lab on a Chip. 2011;11(19):3249-55.
20. Gabardo CM, Zhu Y, Soleymani L, Moran-Mirabal JM. Electrodes: Bench-Top Fabrication of Hierarchically Structured High-Surface-Area Electrodes (Adv. Funct. Mater. 24/2013). Advanced Functional Materials. 2013;23(24):3017-.
21. Chen A, Lieu DK, Freschauf L, Lew V, Sharma H, Wang J, et al. Shrink-Film Configurable Multiscale Wrinkles for Functional Alignment of Human Embryonic Stem Cells and their Cardiac Derivatives. Advanced Materials. 2011;23(48):5785-91.
22. Sidorov AN, Sławiński GW, Jayatissa A, Zamborini FP, Sumanasekera GU. A surface-enhanced Raman spectroscopy study of thin graphene sheets functionalized with gold and silver nanostructures by seed-mediated growth. Carbon. 2012;50(2):699-705.
23. Zhang L, Lang X, Hirata A, Chen M. Wrinkled nanoporous gold films with ultrahigh surface-enhanced Raman scattering enhancement. ACS nano. 2011;5(6):4407-13.
24. Hofmann O, Miller P, Sullivan P, Jones TS, Bradley DD. Thin-film organic photodiodes as integrated detectors for microscale chemiluminescence assays. Sensors and Actuators B: Chemical. 2005;106(2):878-84.
25. Minas G, Wolffenbuttel R, Correia J. A lab-on-a-chip for spectrophotometric analysis of biological fluids. Lab on a Chip. 2005;5(11):1303-9.
26. Sivashankar S, Sapsanis C, Buttner U, Salama KN. Flexible low-cost cardiovascular risk marker biosensor for point-of-care applications. Electron Lett. 2015;51(22):1746-7.
27. Yin D, Deamer DW, Schmidt H, Barber JP, Hawkins AR. Single-molecule detection sensitivity using planar integrated optics on a chip. Optics letters. 2006;31(14):2136-8.
28. Dodge A, Turcatti G, Lawrence I, de Rooij NF, Verpoorte E. A microfluidic platform using molecular beacon-based temperature calibration for thermal dehybridization of surface-bound DNA. Analytical chemistry. 2004;76(6):1778-87.
29. Guttenberg Z, Müller H, Habermüller H, Geisbauer A, Pipper J, Felbel J, et al. Planar chip device for PCR and hybridization with surface acoustic wave pump. Lab on a Chip. 2005;5(3):308-17.
30. Du Y, Wei H, Kang J, Yan J, Yin X-b, Yang X, et al. Microchip capillary electrophoresis with solid-state electrochemiluminescence detector. Analytical chemistry. 2005;77(24):7993-7.
31. Edel JB, Beard NP, Hofmann O, Bradley DD. Thin-film polymer light emitting diodes as integrated excitation sources for microscale capillary electrophoresis. Lab on a Chip. 2004;4(2):136-40.
32. Hofmann O, Wang X, Bradley DD. Towards microalbuminuria determination on a disposable diagnostic microchip with integrated fluorescence detection based on thin-film organic light emitting diodes. Lab on a Chip. 2005;5(8):863-8.
33. Mashraei Y, Sivashankar S, Buttner U, Salama K. Integration of Fractal Biosensor in a Digital Microfluidic Platform. IEEE Sensors Journal. 2016;PP(99):1-.
34. Rogers CI, Qaderi K, Woolley AT, Nordin GP. 3D printed microfluidic devices with integrated valves. Biomicrofluidics. 2015;9(1):016501.
35. Lee KG, Park KJ, Seok S, Shin S, Park JY, Heo YS, et al. 3D printed modules for integrated microfluidic devices. RSC Advances. 2014;4(62):32876-80.
36. Lee MP, Cooper GJ, Hinkley T, Gibson GM, Padgett MJ, Cronin L. Development of a 3D printer using scanning projection stereolithography. Scientific reports. 2015;5.
37. Chan HN, Chen Y, Shu Y, Chen Y, Tian Q, Wu H. Direct, one-step molding of 3D-printed structures for convenient fabrication of truly 3D PDMS microfluidic chips. Microfluidics and Nanofluidics. 2015:1-10.
38. Comina G, Suska A, Filippini D. Low cost lab-on-a-chip prototyping with a consumer grade 3D printer. Lab on a Chip. 2014;14(16):2978-82.
39. Giobbe GG, Michielin F, Luni C, Giulitti S, Martewicz S, Dupont S, et al. Functional differentiation of human pluripotent stem cells on a chip. Nat Meth. 2015;12(7):637-40.
40. Hong C-C, Choi J-W, Ahn CH. A novel in-plane passive microfluidic mixer with modified Tesla structures. Lab on a Chip. 2004;4(2):109-13.
41. Gupta S. Optoelectronic Devices and Systems: PHI Learning Pvt. Ltd.; 2014.
42. Hu J, Wang S, Wang L, Li F, Pingguan-Murphy B, Lu TJ, et al. Advances in paper-based point-of-care diagnostics. Biosensors and Bioelectronics. 2014;54:585-97.

View Article Online
DOI: 10.1039/C6RA13582J

43. Kefala I, Papadopoulos VE, Kokkoris G, Karpou G, Moschou D, Papadakis G, et al. A Passive Micromixer for Bioanalytical Applications. 2014.
44. Jeon NL, Dertinger SK, Chiu DT, Choi IS, Stroock AD, Whitesides GM. Generation of solution and surface gradients using microfluidic systems. Langmuir. 2000;16(22):8311-6.
45. Quan X, Liu H, Lu Z, Quan Y, Wang X, Hu X, et al. Design of stray light suppressed digital micromirror device-based spectrometer with compound parabolic concentrator. OPTICE. 2015;54(11):115101.
46. Shallan AI, Smejkal P, Corban M, Guijt RM, Breadmore MC. Cost-effective three-dimensional printing of visibly transparent microchips within minutes. Analytical chemistry. 2014;86(6):3124-30.
47. Leigh SY, Tattu A, Mitchell JS, Entcheva E. M3: Microscope-based maskless micropatterning with dry film photoresist. Biomedical microdevices. 2011;13(2):375-81.
48. Chen L, Luo G, Liu K, Ma J, Yao B, Yan Y, et al. Bonding of glass-based microfluidic chips at low-or room-temperature in routine laboratory. Sensors and Actuators B: Chemical. 2006;119(1):335-44.
49. Gabriel EFM, Coltro WKT, Garcia CD. Fast and versatile fabrication of PMMA microchip electrophoretic devices by laser engraving. Electrophoresis. 2014;35(16):2325-32.
50. Romoli L, Tantussi G, Dini G. Experimental approach to the laser machining of PMMA substrates for the fabrication of microfluidic devices. Optics and Lasers in Engineering. 2011;49(3):419-27.
51. He Y, Xiao X, Wu Y, Fu J-z. A facile and low-cost micro fabrication material: flash foam. Scientific reports. 2015;5.

View Article Online
DOI: 10.1039/C6RA13582J

Figures

Figure1

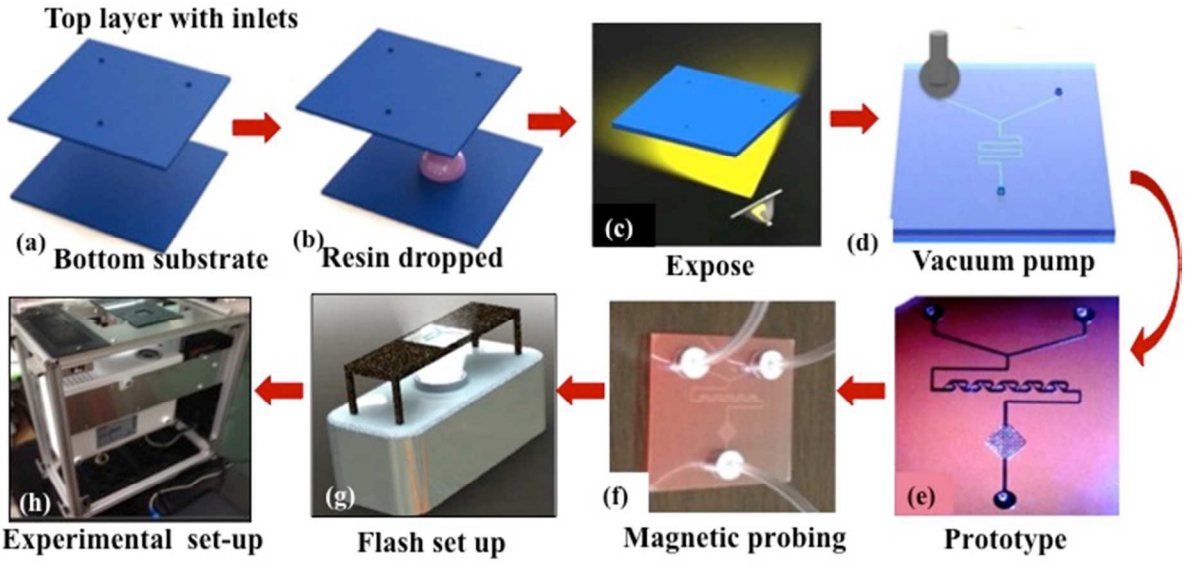

Figure 1- Sequential Fabrication process: (a) cleaned glass with holes drilled on the top glass cover (b) resin placed and spread in between the glass slides (c) resin sandwiched between glass and the projected design is obtained (d) vacuum is applied to inlet and outlets to remove the resin in patterned area (e) prototype of the chip fabricated with pre-drilled inlets and outlet. (f) Magnetic coupling to the FM chip. (g) One-step microfluidic device fabrication method. (h) FM setup with substrate holder

View Article Online
DOI: 10.1039/C6RA13582J

Figure 2

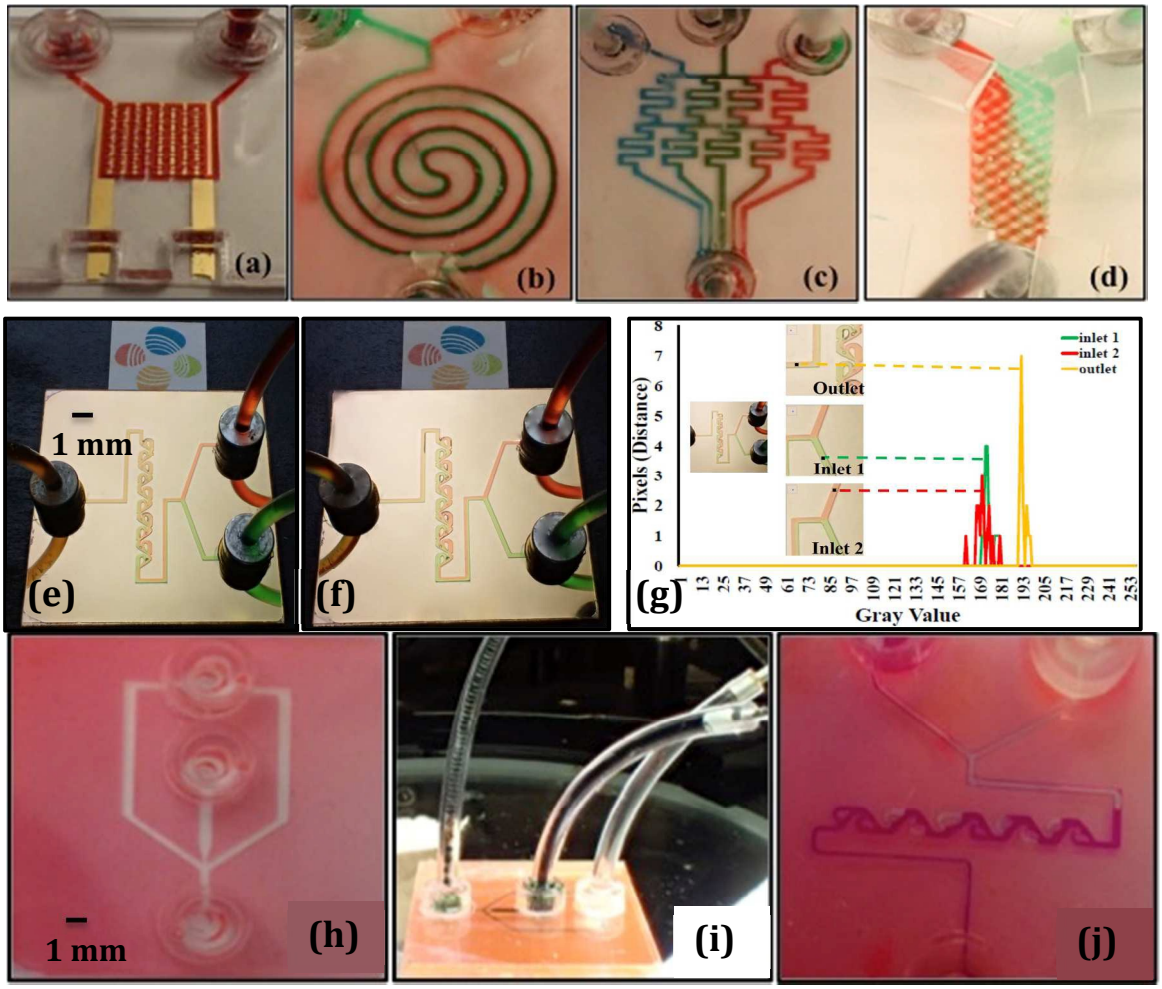

Figure 2: devices that show versatility of the fabrication method. (a) Electronics integrated with microchannels (b) spiral mixer (c) fractal gradient (d) 3D cross flow mixer. (e, f) Illustration of mixing phenomena using a modified tesla mixer fabricated via flash microfluidics and magnetic coupling to inlets and outlet. (e) Shows a flow rate of 0.5ul/min and (f) is at a flow rate of 0.2ul/min (g) Intensity profile at unmixed and mixed regions (h) droplet generator (i) snapshot of droplet generation (j) Chemical reaction within the tesla mixer

View Article Online
DOI: 10.1039/C6RA13582J

Figure 3

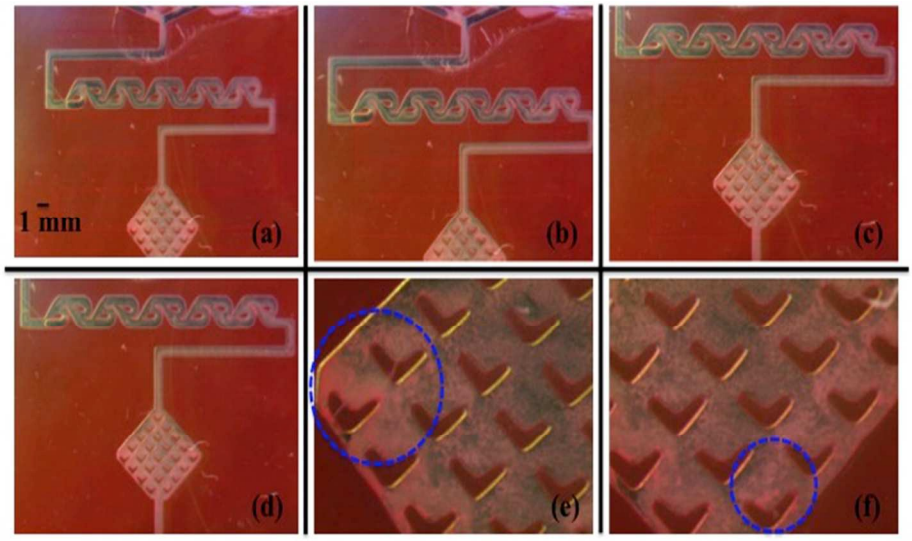

Figure 3- Sequential agglutination process: (a) injection of functionalized beads and analytes (b) the merging of two fluids within the mixers shows trail of the movement. (c) Capturing area filled with antibodies (d) progressing with time clumps being formed in the mixing channel and ahead. (e) Agglutinated clumps held on the V-shaped structures. (f) The clumps settling towards the structure

View Article Online
DOI: 10.1039/C6RA13582J

Figure 4

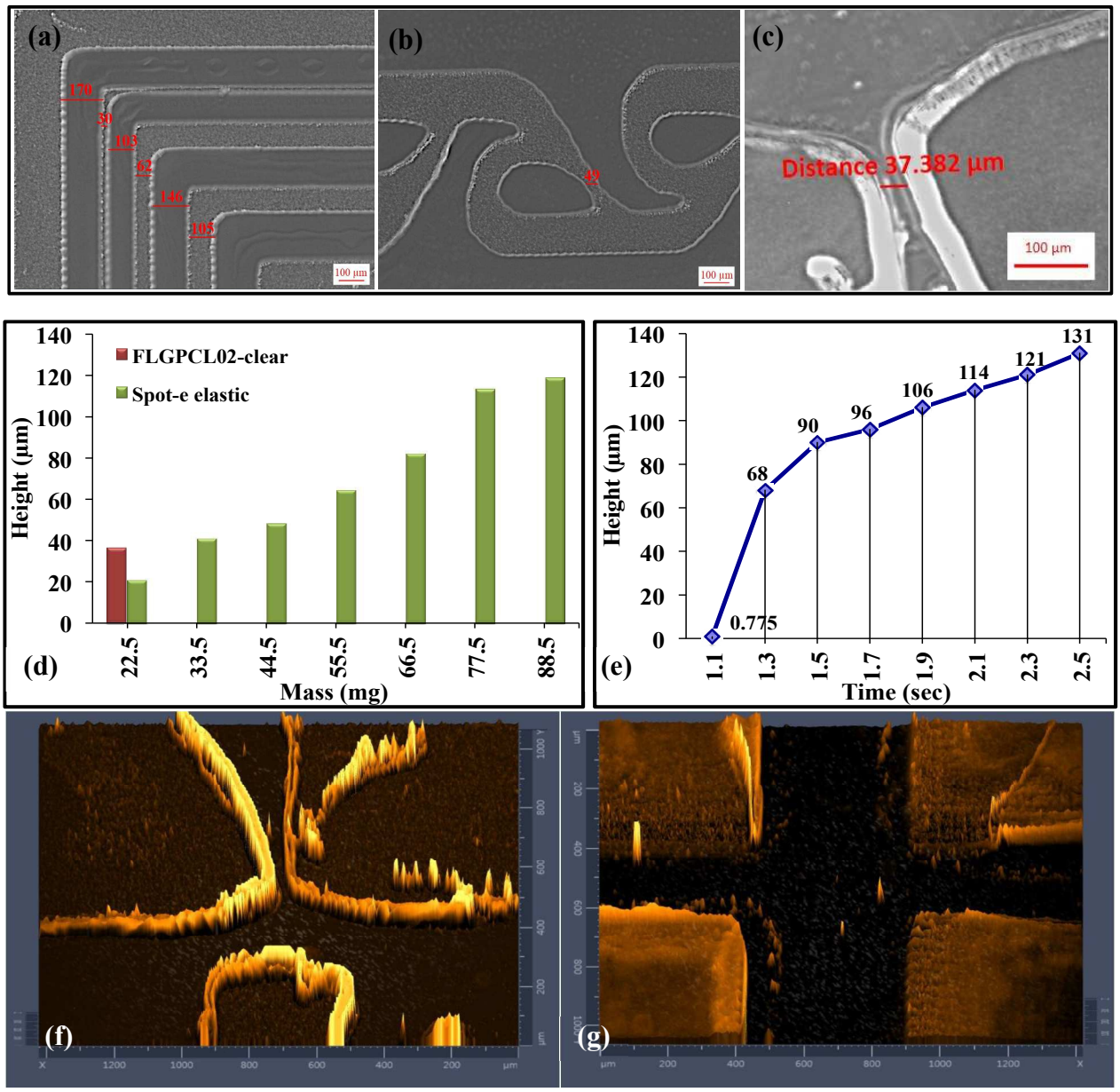

Figure4 (a): Resolution of various sizes of rectangular channels at 3sec exposure on utilizing Spot-E elastic resin. (b): Resolution of Spot-E elastic resin at 3sec exposure of a micromixer (c): Resolution of Spot-E elastic resin at 3sec exposure of a squares at close proximity after bonding the chip. (d) Viscosity dependent Aspect ratio of structures formed with FLGPCL02 and Spot-e elastic resin (e) Resin curing height with change in time (f) profile plot of the channel after bonding the chip (g) profile plot of the channel after exposure.

View Article Online
DOI: 10.1039/C6RA13582J

Figure 5

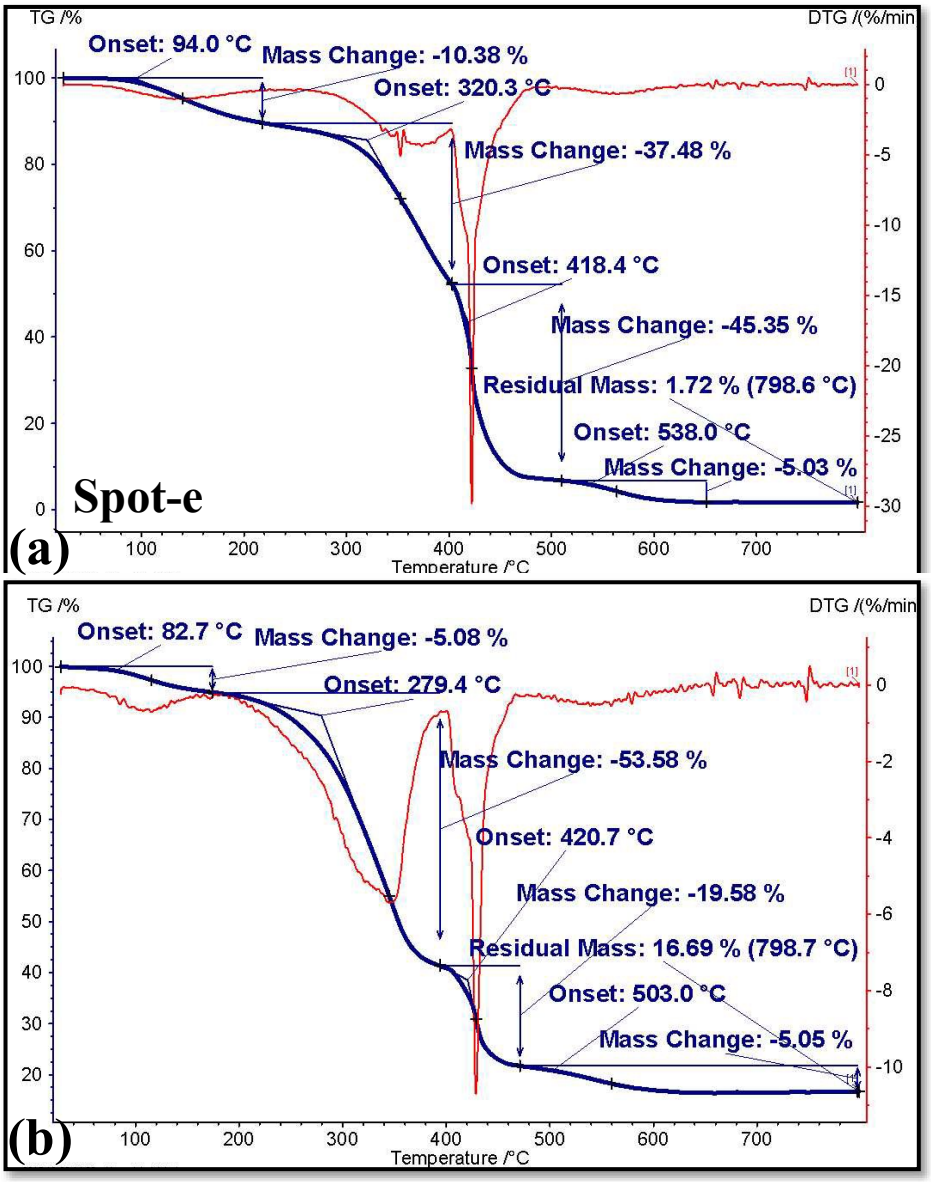

Figure 5- Two proprietary resins Spot-E elastic (a) and FLGPCL02 clear (b) are compared via TGA to identify their thermal properties.

View Article Online
DOI: 10.1039/C6RA13582J

Figure 6

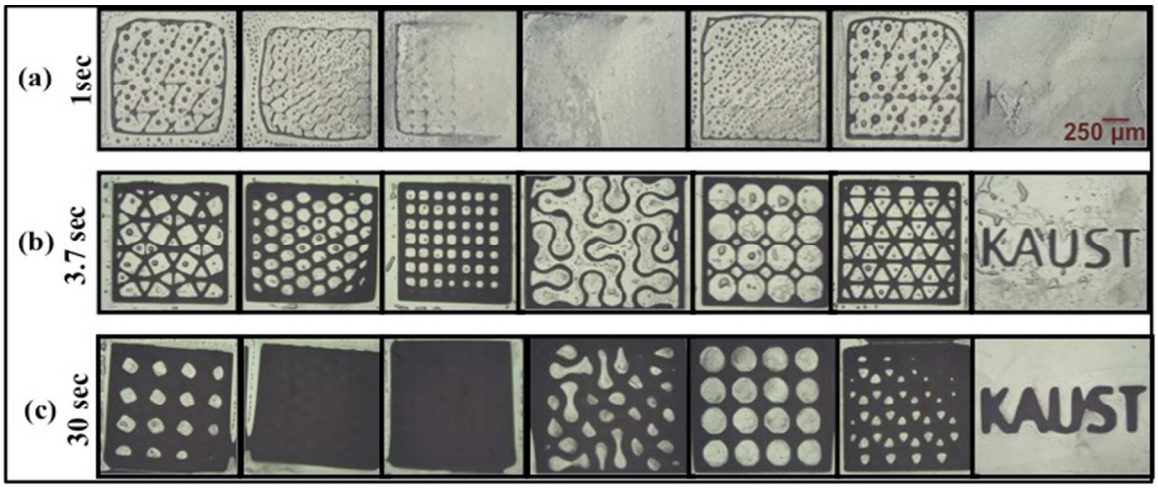

Figure 6- *three cases with different structure at the 3 time intervals to show the UV exposure effects. (a) Under exposed: Feeble features are obtained (b) optimum exposure: to obtain sharp and neat structures (c) overexposed: the structures are merged and unsharpened images are seen.*